J|A|C|S ARTICLES

Published on Web 04/20/2009

Capturing and Analyzing the Excited-State Structure of a Cu(I) Phenanthroline Complex by Time-Resolved Diffraction and Theoretical Calculations

Ivan I. Vorontsov,[†,||] Tim Graber,[‡] Andrey Yu. Kovalevsky,[†,⊥] Irina V. Novozhilova,[†,#] Milan Gembicky,[†] Yu-Sheng Chen,[§,▽] and Philip Coppens*[,†]

Department of Chemistry, State University of New York at Buffalo, Buffalo, New York 14260, University of Chicago, Chicago, Illinois 60637, and University of Toledo, Toledo, Ohio 43606

Received February 5, 2009; E-mail: coppens@buffalo.edu

Abstract: Time-resolved crystallography and density functional theory calculations are used to analyze the geometric and electronic changes that occur upon photoexcitation of $[Cu(I)(dmp)(dppe)]^+$ in crystalline $[Cu(I)(dmp)(dppe)][PF_6]$ [dmp = 2,9-dimethyl-1,10-phenanthroline; dppe = 1,2-bis(diphenylphosphino)-ethane]. In the pump−probe experiment, laser and X-ray pulses are synchronized to capture an image of the instantaneous molecular distortions in the transient triplet state. Parallel theoretical calculations, with the phenyl groups replaced by methyl groups, yield information on the distortion of the isolated cation and the change in electron density upon excitation. The experimental distortions are significantly less than the calculated values and are different for the two independent molecules in the asymmetric unit; these findings are attributed to the constraining influence of the crystal matrix. The calculations indicate that the electron transfer upon excitation is mostly from the dmpe ligand to the dmp ligand, while the Cu atomic charge changes by only $\sim+0.1e$, although the charge distribution on Cu is significantly affected. As found for homoleptic $[Cu(I)(dmp)_2]^+$, the change in the population of the Cu atom is close to the calculated difference between the corresponding Cu(II) and Cu(I) complexes. Charge density difference maps confirm these conclusions and show a large rearrangement of the electron density on the Cu atom upon excitation.

Introduction

Photochemical processes involving charge separation and recombination are generally accompanied by geometry changes in the donor−acceptor system. In addition to the free-energy driving force of the electron transfer, $-\Delta G^0$, and the pre-exponential factor, A, the reorganization energy, λ, is a key quantity in the Marcus theory of electron transfer.[1] As is evident from studies on dyad molecules in liquid crystals,[2−4] the rate of back-transfer is strongly affected by the restraining influence of the matrix in which a charge-separated state is embedded. Thus, a fundamental understanding of photoinduced electron transfer requires knowledge of the geometry changes accompanying the electron transfer process in the molecule in which the charge transfer is taking place. Once the geometry changes are better understood, systems can be designed in which charge recombination is slower, and charge can be stored for longer periods. Time-resolved diffraction techniques[5−9] open the possibility of determining geometry changes upon molecular excitation and can be applied to molecules in different environments if the versatility of supramolecular crystals is exploited.[10]

Time-resolved crystallography at atomic resolution has now proceeded beyond monochromatic X-ray radiation to the use of polychromatic Laue techniques, which allow single-pulse experiments and therefore time resolution better than the microsecond time scale achieved in this study. However, much excited-state (ES) chemistry remains to be explored in the microsecond regime. In our time-resolved study on a binuclear Pt complex,[11,12] only the change in the heavy-atom position

[†] State University of New York at Buffalo.
[‡] University of Chicago.
[§] University of Toledo.
[||] Current address: Department of Biochemistry and Molecular Biophysics, University of Arizona, Tucson, AZ 85721.
[⊥] Current address: Bioscience Division, Group B-8, Los Alamos National Laboratory, Los Alamos, NM 87545.
[#] Current address: Department of Chemistry, Box 68, Middle Tennessee State University, Murfreesboro, TN 37132.
[▽] Current address: ChemMatCARS, Advanced Photon Source, Argonne National Laboratory, Argonne, IL 60439.

(1) Barbara, P. F.; Meyer, T. J.; Ratner, M. A. *J. Phys. Chem.* **1996**, *100*, 13148–13168.
(2) Levanon, H.; Galili, T.; Regev, A.; Wiederrecht, G. P.; Svec, W. A.; Wasielewski, M. R. *J. Am. Chem. Soc.* **1998**, *120*, 6366–6373.
(3) Wiederrecht, G. P.; Svec, W. A.; Wasielewski, M. R. *J. Phys. Chem. B* **1999**, *103*, 1386–1389.
(4) Wiederrecht, G. P.; Svec, W. A.; Wasielewski, M. R.; Galili, T.; Levanon, H. *J. Am. Chem. Soc.* **2000**, *122*, 9715–9722.
(5) Ihee, H.; Rajagopal, S.; Srajer, V.; Pahl, R.; Anderson, S.; Schmidt, M.; Schotte, F.; Anfinrud, P. A.; Wulff, M.; Moffat, K. *Proc. Natl. Acad. Sci. U.S.A.* **2005**, *102*, 7145–7150.
(6) Cole, J. M.; Raithby, P. R.; Wulff, M.; Schotte, F.; Plech, A.; Teat, S. J.; Bushnell-Wye, G. *Faraday Discuss.* **2003**, *122*, 119–129.
(7) Coppens, P.; Novozhilova, I. V. *Faraday Discuss.* **2003**, *122*, 1–11.
(8) Techert, S.; Schotte, F.; Wulff, M. *Phys. Rev. Lett.* **2001**, *86*, 2030–2033.
(9) Coppens, P. *Chem. Commun.* **2003**, 1317–1320.
(10) Zheng, S.-L.; Gembicky, M.; Messerschmidt, M.; Dominiak, P. M.; Coppens, P. *Inorg. Chem.* **2006**, *45*, 9281–9289.
(11) Kim, C. D.; Pillet, S.; Wu, G.; Fullagar, W. K.; Coppens, P. *Acta Crystallogr.* **2002**, *A58*, 133–137.
(12) Novozhilova, I. V.; Volkov, A. V.; Coppens, P. *J. Am. Chem. Soc.* **2003**, *125*, 1079–1087.

10.1021/ja900921p CCC: $40.75

could be determined, in part because of the dominance of the scattering of the Pt atom but also because of technical limitations in the first experiments.[11] Further advances in techniques and methods, implemented at the Advanced Photon Source at Argonne National Laboratory, have made it possible to obtain experimental information on both metal and ligand geometries. The improvements include the considerably higher flux at the third-generation Advanced Photon Source, more efficient delivery of the laser beam to the crystal, improved pulse selectors,[13] and more advanced timing circuitry. We report here an ES diffraction study in which information on both the heavy-atom and ligand geometries has been obtained. A parallel density functional theory (DFT) calculation provides information on the geometry and electron density changes upon excitation expected for the isolated molecule.

Cu(I) diimine coordination complexes undergo metal-to-ligand charge transfer (MLCT) or ligand-to-ligand charge transfer (LLCT) upon excitation, leading to relatively long lifetime excited triplet states,[14] which are significantly distorted relative to the ground-state (GS) complex. They can be used in efficient dye-sensitized solar cells.[15,16] The highly luminescent excited states have powerful reducing properties and can inject electrons into the conduction bands of semiconductors when the complexes are tethered to their surfaces. As a result, the Cu(I) phenanthrolines and related bisdiimines have been extensively investigated using a variety of techniques[5,17−20] following the first studies by McMillin and co-workers.[14,21−23] They emit in the visible region and are reported to have room-temperature triplet ES lifetimes ranging from nanoseconds up to 1.8 μs for $[Cu(dbp)]^{2+}$ (dbp = 2,9-dibutyl-1,10-phenanthroline) at 90 K and in some cases longer at 16−17 K.[24,25]

Replacement of one of the two phenanthroline ligands by bulky phosphine ligands considerably increases the lifetimes of the triplet states relative to those of the homoleptic bisdimethylphenanthrolines.[22,26,27] As described below (see Figure 2), the subject of the current study, [Cu(I)(dmp)(dppe)][PF_6] [dmp = 2,9-dimethyl-1,10-phenanthroline; dppe = 1,2-bis(diphenylphosphino)ethane (Scheme 1)] has a much longer triplet ES lifetime in the crystal at 17 K. It crystallizes in the monoclinic space group $P2_1/c$ (see Table 1). In addition to the ES structure analysis, this study includes determinations of the GS structure at 16 and 90 K. The crystals contain two independent molecules in the asymmetric unit, thus providing the additional opportunity to study the environment dependence of the distortion upon excitation. A preliminary report on this study has been published.[28]

Scheme 1. Structure of the 1,2-Bis(diphenylphosphino)ethane (dppe) Ligand

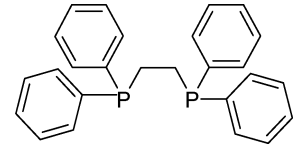

Table 1. Crystallographic Data for [Cu(I)(dmp)(dppe)][PF_6] from the Pump−Probe Experiment

	dark structure	laser-on structure
temperature (K)	16(2)	
wavelength (Å)	0.49594	
crystal system	monoclinic	monoclinic
space group, Z	$P2_1/c$, 8	$P2_1/c$, 8
a (Å)	20.138(3)	20.177(5)
b (Å)	13.595(2)	13.649(4)
c (Å)	26.549(3)	26.542(5)
β (deg)	95.316(6)	95.404(9)
V (Å^3)	7237(2)	7277(5)
D_{calcd} (Mg/m^3)	1.496	
μ (mm^{-1})	0.424	
crystal size (mm^3)	0.04 × 0.05 × 0.04	
θ_{max} (deg)	21.01	
max (sin θ)/λ (Å^{-1})	0.723	0.79
independent reflections	15840	
reflections with $I > 2\sigma(I)$	11252	
completeness (%)	69.2	
data, parameters	15840, 937	
goodness of fit on F^2	1.026	
R1(F) [$I > 2\sigma(I)$]	0.0525	
wR_2(F^2) (all data)	0.0819	
largest diff peak, hole (e/Å^3)	0.849, −0.813	

Experimental Methods

1. Synthesis. $[Cu(CH_3CN)_4][PF_6]$ (100 mg, 0.27 mmol) was added to a degassed acetonitrile solution (50 mL) of dmp·0.5H_2O (58 mg, 0.27 mmol) and dppe (119.5 mg, 0.3 mmol, 10% excess). The color of the solution immediately changed to bright-yellow. The solution was then refluxed for 2 h, after which the solvent was removed under reduced pressure to give a yellow solid. The product was recrystallized from acetonitrile to give [Cu(dmp)(dppe)][PF_6] in 70% yield. Crystals suitable for X-ray diffraction analysis were prepared by slow evaporation of the acetonitrile solution.

2. Spectroscopy. UV−vis absorption spectra were recorded on a PerkinElmer Lambda 35 spectrometer equipped with an integrating sphere for reflectance spectroscopy. The spectra were collected in the 300−1100 nm range at room temperature from freshly drybox-prepared KBr pellets. For the luminescence measurements, a 100 μm single crystal of [Cu(I)(dmp)(dppe)][PF_6] was mounted in a Displex cryogenic cooler equipped with a shroud specially constructed for low-temperature emission spectroscopy. A vacuum chamber with quartz windows attached to the cryostat was evacuated to ~10^{-7} bar. The crystal was cooled to 16 K and excited with λ_{ex} = 366 nm light pulses from a N_2−dye laser with a 1 Hz

(13) Gembicky, M.; Oss, D.; Fuchs, R.; Coppens, P. *J. Synchrotron Radiat.* **2005**, *12*, 665–669.
(14) Rader, R. A.; McMillin, D. R.; Buckner, M. T.; Matthews, T. G.; Casadonte, D. J.; Lengel, R. K.; Whittaker, S. B.; Darmon, L. M.; Lytle, F. E. *J. Am. Chem. Soc.* **1981**, *103*, 5906–5912.
(15) Bessho, T.; Constable, E. C.; Graetzel, M.; Redondo, A. H.; Housecroft, C. E.; Kylberg, W.; Nazeeruddin, M. K.; Neuburger, M.; Schaffner, S. *Chem. Commun.* **2008**, 3717–3719.
(16) Shaw, G. B.; Grant, C. D.; Shirota, H., Jr.; Meyer, G. J.; Chen, L. X. *J. Am. Chem. Soc.* **2007**, *129*, 2147–2160.
(17) Scaltrito, D. V.; Thompson, D. W.; O'Callaghan, J. A.; Meyer, G. J. *Coord. Chem. Rev.* **2000**, *208*, 243–266.
(18) Armaroli, N. *Chem. Soc. Rev.* **2001**, *30*, 113–124.
(19) Iwamura, M.; Takeuchi, S.; Tahara, T. *J. Am. Chem. Soc.* **2007**, *129*, 5248–5256.
(20) Smolentsev, G.; Soldatov, A. V.; Chen, L. X. *J. Phys. Chem. A* **2008**, *112*, 5363–5367.
(21) Everly, R. M.; Ziessel, R.; Suffert, J.; McMillin, D. R. *Inorg. Chem.* **1991**, *30*, 559–561.
(22) Blasse, G.; McMillin, D. R. *Chem. Phys. Lett.* **1980**, *70*, 1–3.
(23) Breddels, P. A.; Berdowski, P. A. M.; Blasse, G.; McMillin, D. R. *J. Chem. Soc., Faraday Trans.* **1982**, *78*, 595–601.
(24) Kovalevsky, A. Y.; Gembicky, M.; Coppens, P. *Inorg. Chem.* **2004**, *43*, 8282–8289.
(25) Kovalevsky, A. Y.; Gembicky, M.; Novozhilova, I. V.; Coppens, P. *Inorg. Chem.* **2003**, *42*, 8794–8802.
(26) Cuttell, D. G.; Kuang, S.-M.; Fanwick, P. E.; McMillin, D. R.; Walton, R. A. *J. Am. Chem. Soc.* **2002**, *124*, 6–7.
(27) Saito, K.; Arai, T.; Takahashi, N.; Tsukuda, T.; Tsubomura, T. *Dalton Trans.* **2006**, 4444–4448.
(28) Coppens, P.; Vorontsov, I. I.; Graber, T.; Kovalevsky, A. Y.; Chen, Y.-S.; Wu, G.; Gembicky, M.; Novozhilova, I. V. *J. Am. Chem. Soc.* **2004**, *126*, 5980–5981.

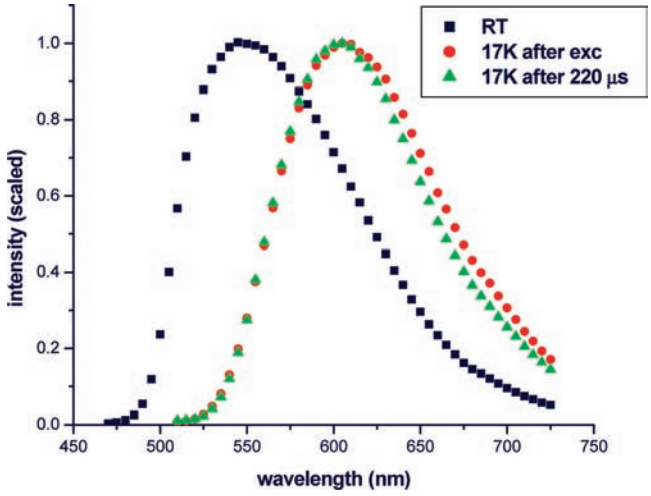

Figure 1. Single-crystal time-integrated emission spectra of [Cu(I)(dmp)(dppe)][PF_6] at (a) room temperature (black ■) and (b) 17 K (red ●, ~1 ns after excitation; green ▲, after 220 μs). Each spectrum was rescaled to an intensity of 1 at its maximum.

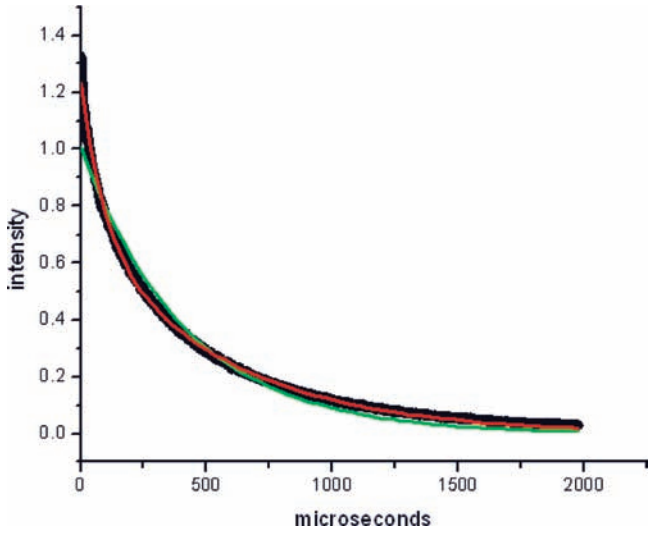

Figure 2. Single-crystal phosphorescence decay of [Cu(I)(dmp)(dppe)][PF_6]. The single-exponential fit is indicated by the green line. The red line shows the double-exponential fit with lifetimes of 87.5 and 551.7 μs. The experimental curve is in black.

repeat frequency. The emission spectrum was passed through an Oriel grating monochromator, recorded with a Hamamatsu photomultiplier tube, and processed by a DSO-2102S computer-based digital oscilloscope with a sampling rate of 100 MHz.

The single-crystal emission spectra of the $[Cu(I)(dmp)(dppe)]^+$ complex at room temperature and 17 K, which are shown in Figure 1, exhibit a broad structureless maximum; a red shift upon cooling is evident. The spectra are similar to those reported for the MLCT transition of the $[Cu(dmp)(PPh_3)_2]^+$ cation.[23,24] Although the shape of the emission spectrum gives no evidence for the existence of two emitting states, the best fit of the time-resolved crystal emission spectrum at low temperature was obtained using a double exponential with exponents of 87.5 and 551.7 μs (Figure 2). The emission is strongly temperature-dependent, as the ES lifetime decreases to 3.9 μs at room temperature and the emission decay becomes monoexponential. A single decay was also observed in the room-temperature emission spectrum of a solution of the complex.

3. Instrumentation for Time-Resolved Crystallography. The experimental arrangement used at the ChemMatCARS 15-ID beamline at the Advanced Photon Source has been described previously.[12] It includes a rapidly rotating chopper wheel acting as a periodic shutter and electronics for synchronizing the X-ray probe and laser pump pulses.

In the pump−probe experiment, each laser pump pulse is synchronized with the X-ray probe pulse, with the latter following the former with an adjustable delay that was set to ~1 ns in the current experiments. In the experiments described here, a 12.8 cm diameter brass chopper wheel with 64 slots, each 1.3 mm in width, was rotated at 5000 rpm to produce ~40 μs X-ray pulses at a frequency of 5333.3 Hz. The X-ray pulse length was selected to be shorter than the lifetime of the studied compound to ensure that the diffraction pattern was recorded before substantial relaxation occurred. On the basis of the 17 K lifetimes of 87.5 and 551.7 μs, the average populations during the 40 μs X-ray pulse were calculated to be 80.3 and 96.5% of the population immediately after excitation, respectively. Light with $\lambda = 355$ nm from a Spectra-Physics T80-YHP70-355Q tripled Nd:YAG pulsed laser was focused on the sample. The laser produced 50 ns pulses at a time-averaged power of 1.4 W at 5 kHz. The number of laser photons per pulse (~5×10^{14}) exceeded the number of molecules in the ~$70 \times 40 \times 40$ μm^3 single crystals used in the experiments.

4. Time-Resolved Data Collection. The monochromatic time-resolved X-ray data collection procedure has been described previously.[29] Data collection using a 0.3° wide scan for each frame while the crystal was exposed to the periodic laser pulses was followed by measurement using the same frame under laser-off conditions.[30] For the laser-on frames, a stroboscopic technique was used in which the data were accumulated in the area detector for a large number of rapidly repeating pump−probe pulse pairs. The laser-off frames were collected under the same conditions except for the absence of the pump pulses. The procedure was repeated for the following frames until data collection was completed or the data quality deteriorated because of the prolonged laser exposure of the sample.

In the current study, each frame was collected for 1 s, corresponding to 5333 laser/X-ray pulses per frame. Fluorescence and X-ray diode detectors were used to control the pump−probe synchronization. Monochromatic radiation with $\lambda = 0.49594$ Å was obtained using a diamond double-crystal monochromator. The crystal temperature was nominally 16 K but (as discussed below) somewhat higher during laser-on data collection. Three successful data sets containing 320, 550, and 300 frames (designated as sets 1, 2, and 3, respectively) were collected. Intensity decay arising from laser damage to the sample was very small for set 1, which was therefore used for the determination of the reference dark structure in the subsequent analysis.

Computational Methods

1. Least-Squares Refinement of the Structural Changes. The scattering formalism, expressed as

$$F_{on}(hkl) = (1 - P)F_{on,GS}(hkl) + PF_{on,ES}(hkl) \qquad (1)$$

where P is the ES population, hkl refers to the set of Miller indices for the reflection, and $F_{on}(hkl)$ is the laser-on structure factor, is based on a random distribution of ES molecules in the crystal. As in our studies of photoexcited transition-metal nitrosyl compounds, in which significantly higher conversion percentages were reached,[31−35] the

(29) Coppens, P.; Vorontsov, I. I.; Graber, T.; Gembicky, M.; Kovalevsky, A. Y. *Acta Crystallogr.* **2005**, *A61*, 162–172.
(30) Fullagar, W. K.; Wu, G.; Kim, C.; Ribaud, L.; Sagerman, G.; Coppens, P. *J. Synchrotron Radiat.* **2000**, *7*, 229–235.
(31) Coppens, P.; Novozhilova, I.; Kovalevsky, A. *Chem. Rev.* **2002**, *102*, 861–884.
(32) Coppens, P.; Fomitchev, D. V.; Carducci, M. D.; Culp, K. *J. Chem. Soc., Dalton Trans.* **1998**, 865–872.
(33) Carducci, M.; Pressprich, M. R.; Coppens, P. *J. Am. Chem. Soc.* **1997**, *119*, 2669–2678.
(34) Kovalevsky, A. Y.; Bagley, K. A.; Coppens, P. *J. Am. Chem. Soc.* **2002**, *124*, 9241–9248.

formalism was supported by the absence of extra diffraction spots and the success of the fitting procedure.[36]

To increase the sensitivity of the experiment, the least-squares minimization procedure was based on the *relative change* in the intensity $I(hkl)$ for each of the Bragg reflections under the external perturbation.[37,38] In this case, the response ratio $\eta(hkl)$ is defined as

$$\eta(hkl) = \frac{I_{on}(hkl) - I_{off}(hkl)}{I_{off}(hkl)} = \frac{F_{on}(hkl)^2 - F_{off}(hkl)^2}{F_{off}(hkl)^2} \quad (2)$$

where $F_{on}(hkl)^2$ and $F_{off}(hkl)^2$ are the laser-on and laser-off squared structure factors, respectively.

The laser heat generated during exposure of the crystal to the laser pulses was dissipated through helium-gas cooling of the crystal, especially during the detector readout period. As a result, the sample temperature may have differed during the laser-on and laser-off data collection periods. This effect was taken into account in the data analysis by the introduction of a temperature scale factor k_B multiplying the atomic displacement parameters of the reference GS in the ES refinement.

The response-ratio least-squares refinement program used, Laser03, is a considerably revised variant of earlier software.[39] It allows refinement of ES populations of each of the data sets and of the position and orientation of rigid-body fragments of both the GS and ES complexes. The rigid-body option becomes essential when large complexes are studied, as is the case in the work described here.

2. DFT Calculations of the Ground and Excited States. Calculations with the ADF suite of programs[40−42] were performed on $[Cu(I)(dmp)(dmpe)]^+$ [dmpe = 1,2-bis(dimethylphosphino)ethane], in which the phenyl groups of the title compound were replaced by methyl groups because of computational limitations. This substitution was not expected to have a significant effect on the conclusions, as both methyl and phenyl are electron-donating groups. The generalized gradient approximation (GGA) with the B88LYP functional was used. The atomic orbitals of copper were described by a triple-ζ Slater-type basis set (ADF database TZP), while for the carbon, nitrogen, phosphorus, and hydrogen atoms, a double-ζ Slater-type basis set with one polarization function (ADF database DZP) was employed. The $(1s2s2p)^{10}$ core shells of Cu and P and the $(1s)^2$ core shells of C and N were treated by the frozen-core approximation. Relativistic effects were taken into account using the zeroth-order regular approximation (ZORA). No symmetry constraints were imposed on the molecule. The geometry convergence threshold for the Cartesian gradients was set to 10^{-4} hartree/Å. The integrals were evaluated numerically with an accuracy of 8 significant digits. All of the optimized molecular geometries were confirmed as true energy minima by observation of only positive eigenvalues in the Hessian matrices. The T_1 ES was defined by HOMO-to-LUMO promotion of an electron and fixing of the multiplicity. The choice of this state was supported by the calculated energy differences, as described below. Molecular properties were calculated with the ADF auxiliary program DENSF. All of the graphical representations were created using MOLEKEL4.1.

Table 2. Results from Data Analysis and Response-Ratio Refinement[a]

	set 1	set 2	set 3
$2\Delta B^{WP}$	0.99	1.22	0.61
k_B^{WP} (U_{av} = 0.007)	1.90	2.10	1.55
ES population	0.097(2)	0.073(2)	0.085(5)
		all data	
R(η)		0.2654	
wR(η)		0.3552	
GOF		1.9918	
N_{par}		25(ES) + 24(GS) = 49	
N_{obs} with $\eta > 2\sigma(\eta)$		9154	

[a] Definitions: WP indicates a value obtained from a Wilson plot; k_B is the temperature scale factor described in the text; $R(\eta) = \Sigma|\eta_{calcd} - \eta_{exptl}|/\Sigma|\eta_{exptl}|$; $wR(\eta) = [\Sigma|w(\eta_{calcd} - \eta_{exptl})|^2/\Sigma|w\eta_{exptl}|^2]^{1/2}$; $GOF = [\Sigma|w(\eta_{calcd} - \eta_{exptl})|^2/(N_{ref} - N_{par})]^{1/2}$.

Photocrystallographic Analysis

1. Ground-State Structure. The intensity data were integrated, scaled, sorted, and averaged using the SAINT software package.[43] The structure was solved by the direct method using SHELXTL 5.10[44] and refined by full-matrix least-squares against F^2. Non-hydrogen atoms were refined anisotropically. Positions of hydrogen atoms were calculated geometrically and refined isotropically using a riding model with $U_{iso} = 1.2U_{eq}$ ($1.5U_{eq}$ for methyl groups), where U_{eq} is the value for the connected non-hydrogen atom. Crystallographic information is given in Table 1.

2. Estimate of the Temperature Change upon Laser Illumination. To obtain an estimate of the increase in sample temperature during laser exposure for each of the data sets, $\ln(I_{on}/I_{off})$ was plotted versus $[(\sin\theta)/\lambda]^2$, in analogy to the Wilson plot widely used in crystallographic analysis to obtain a first estimate of the isotropic temperature parameters.[45] The slope of the curve equals $-2\Delta B$, where ΔB is an estimate of the difference between the laser-on and laser-off atomic displacement parameters. In terms of U_{av}, the isotropic mean-square displacement parameter in the laser-off structure obtained by averaging over the heavier Cu and P atoms in the structure, the temperature scale factor k_B is given by $k_B = 1 + \Delta B/B_{av}$, where $B_{av} = 8\pi^2 U_{av}$. For the GS structure, $U_{av} = 0.007$ Å^2, which gives k_B values of 1.55−2.10 for the three data sets (Table 2). However, the ΔB values contain a finite contribution from the disorder generated in the crystal by the creation of ES molecules. To estimate this contribution, calculations were performed on a set of model structure factors of the title compound with an ES population of 7% and displacements similar to those found in the current experiment. About 20% of the increase in k_B above 1 was found to be due to the induced disorder, and the k_B values used in the refinement were reduced accordingly.

3. Consistency of the Data Sets. To test the consistency of the response ratios obtained from the three data sets, two correlation plots, η^{set1} versus η^{set2} and η^{set1} versus η^{set3}, were

(35) Kovalevsky, A. Y.; Bagley, K. A.; Cole, J. M.; Coppens, P. *Inorg. Chem.* **2003**, *42*, 140–147.
(36) Vorontsov, I. I.; Coppens, P. *J. Synchrotron Radiat.* **2005**, *12*, 488–493.
(37) Coppens, P. *Synchrotron Radiation Crystallography*; Academic Press Limited: London, 1992.
(38) van Reeuwijk, S. J.; Puig-Molina, A.; Graafsma, H. *Phys. Rev. B* **2000**, *62*, 6192–6197.
(39) Ozawa, Y.; Pressprich, M. R.; Coppens, P. *J. Appl. Crystallogr.* **1998**, *31*, 128–135.
(40) te Velde, G.; Bickelhaupt, F. M.; van Gisbergen, S. J. A.; Fonseca Guerra, C.; Baerends, E. J.; Snijders, J. G.; Ziegler, T. *J. Comput. Chem.* **2001**, *22*, 931–967.
(41) Fonseca Guerra, C.; Snijders, J. G.; te Velde, G.; Baerends, E. J. *Theor. Chem. Acc.* **1998**, *99*, 391–403.
(42) *ADF2002.01*; Scientific Computing & Modelling NV: Amsterdam, 2002; http://www.scm.com.
(43) *SMART and SAINTPLUS: Area Detector Control and Integration Software*, version 6.01; Bruker AXS: Madison, WI, 1999.
(44) *SHELXTL: An Integrated System for Solving, Refining and Displaying Crystal Structures from Diffraction Data*, version 5.10; Bruker AXS: Madison, WI, 1997.
(45) Wilson, A. J. C. *Nature* **1942**, *150*, 152.

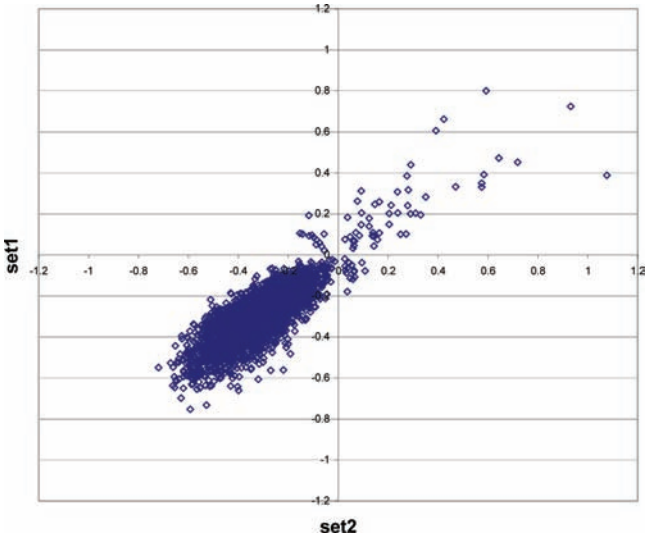

Figure 3. Correlation between response ratios from data sets 1 and 2.

constructed; the former of these is shown in Figure 3. Both plots show a good correlation between the independent measurements, with concentrations in the (−,−) quadrant, where the temperature increase outweighs the structural changes, and in the (+,+) quadrant, where the opposite is true for the less temperature sensitive low-order reflections.

4. Cell Dimensions. The laser-on and laser-off subsets were integrated separately with the standard SAINT PLUS software package.[43] As the unit cell parameters of the three subsets were equal within experimental error, with average discrepancies below 3σ, those of set 1, which were close to the average, were adopted in the analysis. While *a* and *b* increased upon heating, *c* remained essentially constant, in agreement with the results of separate dark-structure measurements at 16 and 90 K (see the Supporting Information).

5. Photodifference Maps. The *photodifference* electron density map, $\Delta\rho(\mathbf{r})$, is defined as the difference between the electron densities after and prior to excitation. It is obtained by a difference Fourier series over the structure factors $F(\mathbf{H})$, where $\mathbf{H}$ is the vector representing the Miller indices *hkl* of an individual reflection:

$$\Delta\rho(\mathbf{r}) = \frac{1}{V_{\text{cell}}}\sum_{\mathbf{H}} [F_{\text{on}}(\mathbf{H}) - F_{\text{off}}(\mathbf{H})] \exp(-2\pi i \mathbf{H}\cdot\mathbf{r}) \quad (3)$$

Photodifference maps in the CuPP planes of the two independent molecules in the asymmetric unit (Figure 4) show large electron density peaks and troughs near the Cu and P atoms, indicating changes of their positions upon excitation. The features are similar to those found near the Pt atom in our earlier study of $[Pt_2(pop)_4]^{4-}$, in which a Pt displacement of ∼0.3 Å was observed. The photodifference maps were used to provide starting parameters for the ES structure refinement.

6. Excited-State Least-Squares Analysis. The reference structure used in the analysis was the GS structure from the laser-off data transferred to the slightly different laser-on unit cell. The initial values of the ES populations in the three experiments, obtained from the separate refinements of the data sets, were kept constant during the initial refinements of the global data set but included in the final cycles of the refinement, the results of which are listed in Table 2. The populations were in the 7−10% range, which is considerably higher than the ∼2% ES populations achieved in the ES analysis of the Pt(pop) complex.

A total of 25 ES and 24 GS parameters were refined against 9154 unique response ratios. For both the GS and ES, each of the ligands was refined as part of a rigid body centered on the appropriate Cu atom. In addition, the ES ligands were allowed to rotate along three perpendicular axes through the Cu atom position and to translate along the local twofold axis through the appropriate Cu atom and bisecting the ligand.

The translations of the GS components were in the 0.01−0.04 Å range (average 0.02 Å), while the rigid body rotations of the not-converted molecules were found to be 0.1−0.3° for the $[Cu(dmp)(dppe)]^+$ ions and somewhat larger (but not exceeding 1°) for the PF_6 ions, which are relatively free to rotate within their almost spherical envelopes.

Discussion of Results and Comparison with Theory

The changes in the Cu coordination bond lengths were obtained from the rigid-body refinement of the ligands and are listed in Table 3, together with the GS distances and the values from the theoretical calculations, which gave an energy difference of 2.47 eV, corresponding to ∼500 nm, which is in reasonable agreement with the low-temperature emission spectrum in Figure 1. For the Cu−P distances, an average increase of 0.028(5) Å was obtained, which is equal to the theoretical value of 0.018 Å within experimental error. The standard deviations in the Cu−N distances were too large to arrive at a conclusion.

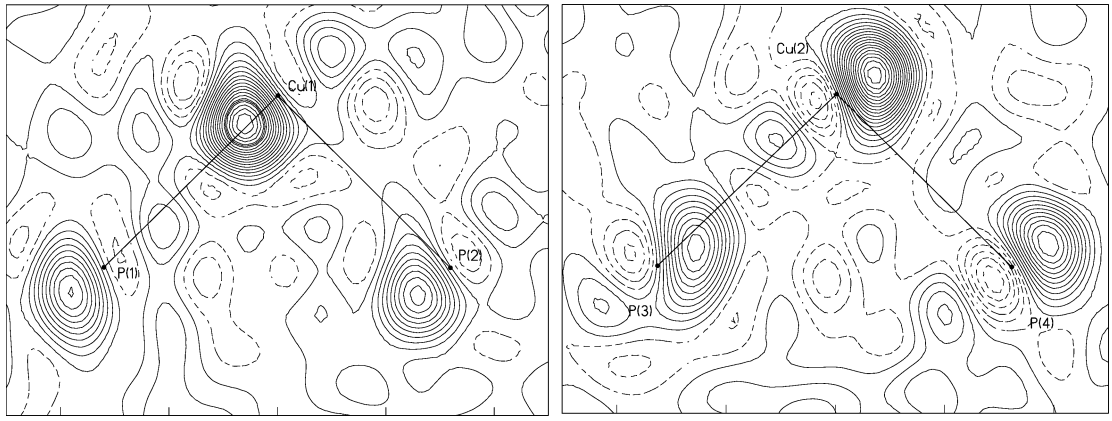

Figure 4. Photodifference maps in the GS CuPP planes (set 1 data): (a) molecule 1; (b) molecule 2. The contour interval is 0.4 e/Å^{-3}, and dashed contours represent negative values.

Table 3. Bond Lengths and Angles in the GS and ES of [Cu(dmp)(dppe)]$^+$ (from Experiment) and [Cu(dmp)(dmpe)]$^+$ (from Theory, C_1 Symmetry) and Calculated Energies

	GS			ES				
	expt			expt			Δ(ES − GS)	
	mol 1	mol 2	theory	mol 1	mol 2	theory	expt (av)	theory
				Bond Lengths (Å)				
Cu−N1	2.030(3)	2.063(3)	2.070	2.04(2)	2.04(2)	1.990	0.00(1)	−0.081
Cu−N2	2.077(2)	2.068(2)	2.079	2.09(2)	2.05(2)	1.997		
Cu−P1	2.244(1)	2.274 (1)	2.256	2.29(1)	2.29(1)	2.274	+0.028(5)	+0.018
Cu−P2	2.237(1)	2.256 (1)	2.258	2.28(1)	2.27(1)	2.276		
				Bond Angles (deg)				
N−Cu−N	82.5(1)	81.9(1)	80.8	82.0(6)	82.9(7)	84.9	+0.2(4)	+4.1
P−Cu−P	90.99(3)	91.42(3)	92.6	88.7(3)	90.6(3)	89.5	−1.6(2)	−3.1
				Calculated Energies				
E (hartree)	−		−11.5263			−11.4358		+0.0905
E (eV)	−		−313.65			−311.18		+2.47

The most pronounced shifts upon excitation occurred for the Cu atoms, which moved in the unit cell by 0.26(2) and 0.28(2) Å in the two independent molecules 1 and 2, respectively. The attached phosphorus atoms moved in the same direction, as is evident in the photodifference maps (Figure 4). The overall change of the molecules in the lattice is illustrated in Figure 5. The conformation of the Cu(I) diimines can be described in terms of the intramolecular interligand dihedral angle and the rocking and wagging angles of the ligands, following White and co-workers.[46] The angles θ_x, θ_y, and θ_z (Figure 6) are 90° in the idealized D_{2d} symmetry of the Cu(I) complexes but deviate from this value as the distortion from D_{2d} symmetry increases. The experimental values are listed in Table 4 for the GS and ES together with those calculated for the two states of [Cu(I)(dmp)(dmpe)]$^+$ and for the GS of [Cu(II)(dmp)(dmpe)]$^{2+}$. The deviations of θ_x, θ_y, and θ_z from 90° correspond to the rocking, wagging, and flattening motions of the molecule, respectively.

In both independent molecules in the crystal, the rocking distortion, $(90° - \theta_x)$, decreased to a value of 0.4(5)°, not significantly different from zero, in agreement with the decrease from 2.2 to 0.6° calculated with DFT for the reference complex, the isolated [Cu(I)(dmp)(dmpe)]$^+$ ion. The wagging distortion, defined by $(90° - \theta_y)$, similarly decreased to very small values in molecule 1 [1.4(5)°] and in the isolated reference molecule but remained essentially constant at the nonzero value of ∼5° in molecule 2. According to theory, the rocking and wagging distortions were also absent in the GS of Cu(II)(dmp)(dmpe)$^{+2}$, but a considerable flattening was observed (see the last three rows of Table 4).

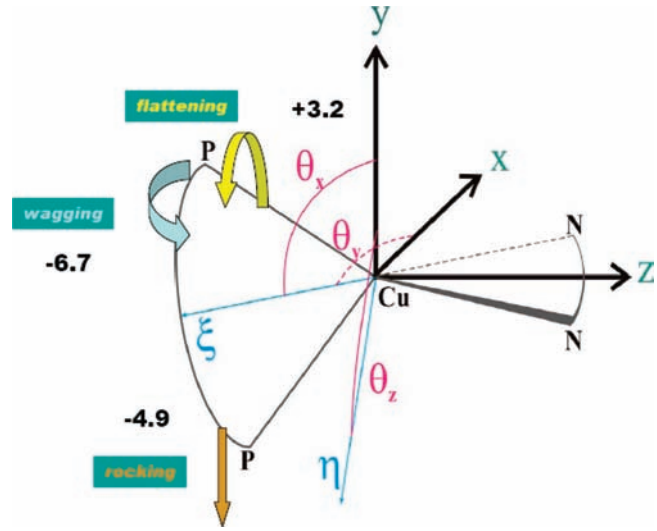

Figure 6. Schematic representation of the distortions in molecule 1 of the [Cu(I)(dmp)(dppe)]$^+$ complex in the crystal, in terms of the distortions defined by White and co-workers for Cu(dmp)$_2$ complexes (ref 46). The angles θ_x, θ_y, and θ_z describe the rocking, wagging, and flattening distortions, respectively. The coordinate system is chosen to place triangle N−Cu−N in the *xz* plane. The unit vector ξ bisects the P−Cu−P angle, and the unit vector η is perpendicular to the P−Cu−P plane. Full numerical details are give in Table 4.

The flattening upon excitation, i.e. the change in the deviation of θ_z from 90°, which was more than 30° in the isolated [Cu(I)(dmp)$_2$]$^+$ complex[47] and calculated to be 8° for the isolated

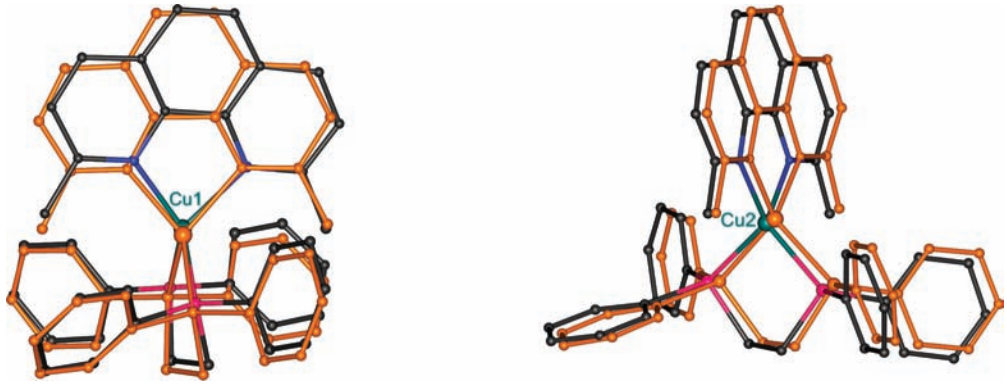

Figure 5. ES geometries of the two independent molecules (orange) superimposed on the GS of the complex (Cu, green; C, black; P, purple; N, blue). Slightly different views are shown to illustrate the change in rocking distortion (left) and the displacement of the phenanthroline ligand from its GS plane (molecule 2, right) upon excitation.

Table 4. Angular Distortions (deg) upon Excitation from Experiment and Theory

angle[a]	GS	ES	Δ(ES − GS)
	Experiment, Molecule 1		
θ_x	94.5(1)	89.6(5)	−4.9
θ_y	95.3(1)	88.6(5)	−6.7
θ_z	90.5(1)	93.7(5)	+3.2
	Experiment, Molecule 2		
θ_x	95.6(1)	90.4(5)	−5.2
θ_y	84.1(1)	85.1(5)	+1.0
θ_z	92.8(1)	92.7(5)	−0.1
	Theory, Cu(I) Complex		
θ_x	92.2	90.6	−1.6
θ_y	91.7	90.1	−1.6
θ_z	93.8	101.8	8.0
	Theory, Cu(II) Complex		
θ_x	90.2		
θ_y	90.1		
θ_z	105.4		

[a] θ_x, θ_y, and θ_z describe the rocking, wagging, and flattening distortions, respectively.

$[Cu(I)(dmp)(dmpe)]^+$ ion, was only 3.2(5)° in molecule 1, whereas no further flattening was observed for molecule 2. It should be noted that the second molecule was already flattened by 2.8(1)° in the GS, indicating a significant constraint of the molecular conformation even in the GS. The lack of further flattening of molecule 2 and the modest flattening of molecule 1 in the crystal compared with the calculated isolated-molecule value attest to the constraining influence of the crystalline matrix upon photoexcitation. This is most striking for molecule 2, which showed a decrease only in the rocking distortion upon excitation. It is tempting to relate the different behavior of the two independent molecules to the double-exponential decay of the emission observed at low temperatures. An alternative explanation citing the involvement of two triplet states, which must be closely spaced given the lack of structure in the emission spectra, is not supported by the calculations on the isolated molecule or the single decay observed in the room-temperature emission experiment.

Though it is not possible to give a reliable quantitative estimate of the reorganization energy λ from the current results, as the ligands were treated as rigid bodies in the analysis, the drastic reduction in the change in the distortion angles upon excitation implies a much diminished value of λ in the crystalline phase and points to an intrinsic difference between the solution- and crystalline-state photochemistries.

A large decrease in reorganization energy upon immobilization has been observed in other cases. It is, for example, also apparent from resonance Raman analysis of the photosensitizer dye *cis*-bis(4,4′-dicarboxy-2,2′-bipyridine)bis(thiocyanato)ruthenium(II) adsorbed on a TiO_2 surface.[48] In the latter case, the molecule is anchored to the surface through the carboxylate groups rather than fully embedded in a three-dimensional environment, so differences may be expected. Nevertheless, the reduction in distortion upon excitation is not unexpected.

Electron Density Changes upon Excitation

As experimental mapping of the electron density changes upon excitation is beyond current capabilities, parallel theoretical calculations were performed to investigate the nature of the charge migration. The deformation densities in the Cu(dmp) plane before and after excitation are shown in Figure 7. Although the total charge on the Cu atom was little affected, a pronounced change in the charge density on this atom is evident in the figure. In the tetrahedral Cu(I) GS, the density lobes point toward the ligand atoms, but in the flattened ES, the positive lobes point into the voids between the ligands, a situation quite similar to that observed experimentally for Cu(II) compounds.[49]

The electron migration upon excitation is illustrated in Figure 8. In this figure, the ES density is plotted on the GS molecular frame to eliminate the otherwise dominant contribution from the atomic displacements. Upon charge transfer, the charge migrates mostly to the proximal atoms of the dmp ligand, which gains 0.45e. According to the Mulliken population analysis (Table 5), this gain does not come principally from the Cu atom, which loses only 0.12e, whereas the dmpe ligand, and especially the phosphorus atoms, are depleted by a total of 0.33e, leading to a reduction of the dmp ligand by 0.45e. This conclusion is not affected by a different choice of population analysis, as the Hirshfeld charge shifts are very similar: +0.10 for Cu, −0.29 for dmpe and +0.40 for the dmp ligand. Thus, the excitation

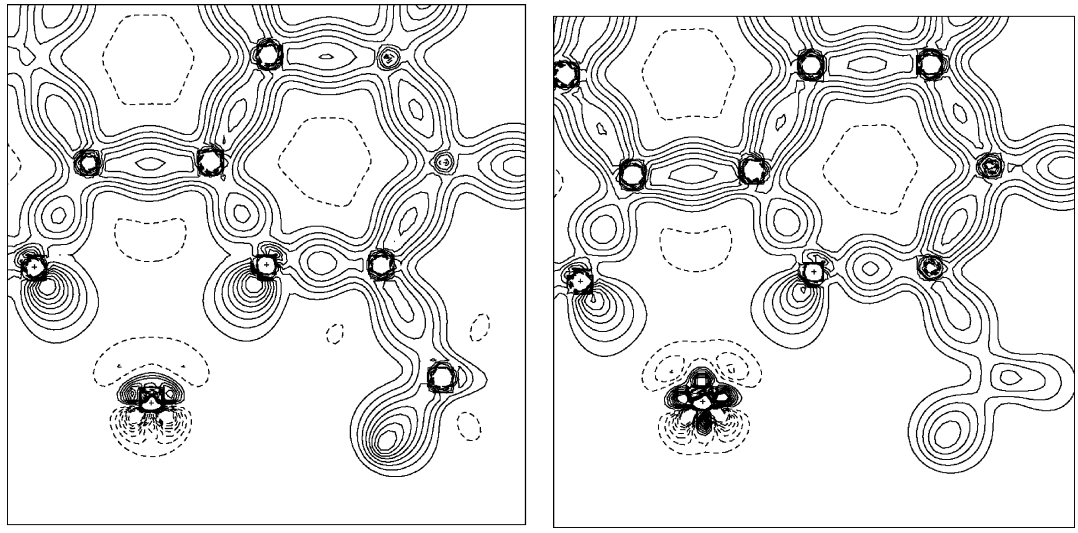

Figure 7. Deformation electron densities of $[Cu(I)(dmp)(dppe)]^+$ in the Cu(dmp) plane (left) before and (right) after excitation. The contour interval is 0.1 e/Å^3, and dashed contours represent negative values.

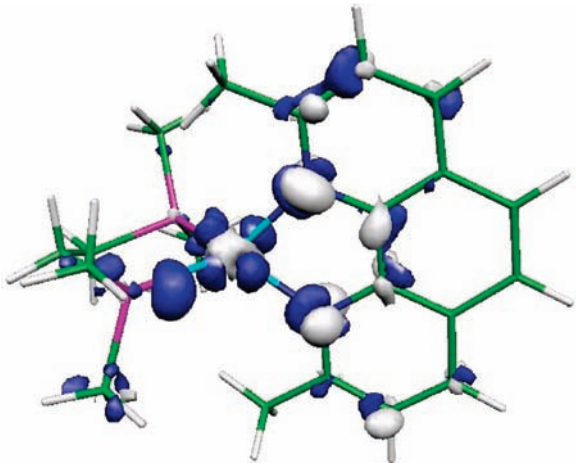

Figure 8. Excitation difference map showing the electron density migration upon excitation to the triplet state. The ±0.005 au (0.034 e/Å^3) isosurfaces are shown (blue surfaces negative, gray surfaces positive). To eliminate the effect of atomic displacement opon excitation, the ES wave function has been transferred to the GS geometry.

Table 5. Theoretical Electron Populations in the GS and ES of [Cu(I)(dmp)(dmpe)]$^+$ and the GS of [Cu(II)(dmp)(dmpe)]$^{2+}$

	Cu	dmpe	dmp	dmpe + dmp
		Total		
GS(I)	18.94	49.36	77.71	127.06
ES(I)	18.82	49.02	78.16	127.18
GS(II)	18.84	47.85	78.31	126.16
		Differences		
ES(I) − GS(I)	−0.12	−0.33	0.45	0.12
GS(II) − GS(I)	−0.09	−1.51	0.60	−0.91
GS(II) − ES(I)	0.03	−1.17	0.14	−1.03

involves mostly LLCT, although, as shown below, a significant change in the charge distribution on the Cu atom occurs.

(46) Dobson, J. F.; Green, B. E.; Healy, P. C.; Kennard, C. H. L.; Pakawatchai, C.; White, A. H. *Aust. J. Chem.* **1984**, *37*, 649–659.
(47) Chen, L. X.; Shaw, G. B.; Novozhilova, I.; Liu, T.; Jennings, G.; Attenkofer, K.; Meyer, G. J.; Coppens, P. *J. Am. Chem. Soc.* **2003**, *125*, 7022–7034.
(48) Shoute, L. C. T.; Loppnow, G. R. *J. Am. Chem. Soc.* **2003**, *125*, 15636–15646.
(49) Coppens, P.; Iversen, B.; Larsen, F. K. *Coord. Chem. Rev.* **2005**, *249*, 179–195.

The comparison with the [Cu(II)(dmp)(dmpe)]$^{2+}$ cation (Table 5) is instructive. The difference between the Cu(II) and Cu(I) GS populations in the optimized structures is only 0.09e, and thus, the change upon oxidation of the Cu atom is essentially equal to the electron change upon excitation. This result is similar to that obtained in DFT calculations on the homoleptic Cu(dmp)$_2$ cations.[47] However, the depletion of electron density on the dmpe ligand upon oxidation is pronounced. It loses 1.5e while the dmp ligand gains 0.60e upon oxidation. Thus, the electron loss upon both oxidation and excitation is essentially confined to the dmpe ligand, while the dmp ligand actually gains electron density.

Conclusions

The results provide quantitative evidence for the strong influence of the crystal environment on molecular rearrangement upon excitation. It is doubtful that flattening distortions as large as 30°, calculated for [Cu(I)(dmp)$_2$]$^+$ are ever achieved for a Cu(I) complex in a crystalline environment, thus implying a significant decrease in the molecular reorganization energy due to the constraints imposed by the medium.

The calculations indicate that the charge transfer in the complex cannot easily be described by labels such as MLCT or LLCT. The latter label seems more appropriate, but it ignores the pronounced electron redistribution on the Cu atom. Most of the charge transfer occurs from the dmpe ligand, in contrast to the situation in the homoleptic [Cu(I)(dmp)$_2$]$^+$ complex, in which the equivalency of the ligands eliminates the possibility of LLCT.

Acknowledgment. The 15-ID beamline is funded by the National Science Foundation (CHE0087817). Financial support of this research by the U.S. Department of Energy (DE-FG02-02ER15372) is gratefully acknowledged. Use of the Advanced Photon Source was supported by the U.S. Department of Energy, Office of Basic Energy Sciences, under Contract W-31-109-ENG-38. We thank Prof. F. V. Bright and co-workers for the measurement of the emission decay in solution.

Supporting Information Available: Crystallographic data for the structures at 16 and 90 K (CIF) and Table S1 listing the fractional coordinates of the GS and ES atoms. This material is available free of charge via the Internet at http://pubs.acs.org.

JA900921P